Detection of [OIII]$_{88\mu m}$ in JADES-GS-z14-0 at z=14.1793

Sander Schouws,[1] Rychard J. Bouwens,[1] Katherine Ormerod,[2] Renske Smit,[2] Hiddo Algera,[3,4]
Laura Sommovigo,[5] Jacqueline Hodge,[1] Andrea Ferrara,[6] Pascal A. Oesch,[7,8,9] Lucie E. Rowland,[1]
Ivana van Leeuwen,[1] Mauro Stefanon,[1] Thomas Herard-Demanche,[1] Yoshinobu Fudamoto,[10] Huub Röttgering,[1]
and Paul van der Werf[1]

[1]Leiden Observatory, Leiden University, NL-2300 RA Leiden, Netherlands
[2]Astrophysics Research Institute, Liverpool John Moores University, 146 Brownlow Hill, Liverpool L3 5RF, United Kingdom
[3]Hiroshima Astrophysical Science Center, Hiroshima University, 1-3-1 Kagamiyama, Higashi-Hiroshima, Hiroshima 739-8526, Japan
[4]National Astronomical Observatory of Japan, 2-21-1, Osawa, Mitaka, Tokyo, Japan
[5]Center for Computational Astrophysics, Flatiron Institute, 162 Fifth Avenue, New York, NY 10010, USA
[6]Scuola Normale Superiore, Piazza dei Cavalieri 7, 50126 Pisa, Italy
[7]Departement d'Astronomie, Université de Genéeve, 51 Ch. des Maillettes, CH-1290 Versoix, Switzerland
[8]Cosmic Dawn Center (DAWN), Copenhagen, Denmark
[9]Niels Bohr Institute, University of Copenhagen, Jagtvej 128, DK-2200 Copenhagen N, Denmark
[10]Center for Frontier Science, Chiba University, 1-33 Yayoi-cho, Inage-ku, Chiba 263-8522, Japan

ABSTRACT

We report the first successful ALMA follow-up observations of a secure $z > 10$ JWST-selected galaxy, by robustly detecting (6.6σ) the [OIII]$_{88\mu m}$ line in JADES-GS-z14-0 (hereafter GS-z14). The ALMA detection yields a spectroscopic redshift of $z = 14.1793\pm0.0007$, and increases the precision on the prior redshift measurement of $z = 14.32^{+0.08}_{-0.20}$ from NIRSpec by $\gtrsim 180\times$. Moreover, the redshift is consistent with that previously determined from a tentative detection (3.6σ) of CIII]$_{1907,1909}$ ($z = 14.178\pm0.013$), solidifying the redshift determination via multiple line detections. We measure a line luminosity of $L_{\text{[OIII]}88} = (2.1 \pm 0.5) \times 10^8 L_\odot$, placing GS-z14 at the lower end, but within the scatter of, the local $L_{\text{[OIII]}88}$-star formation rate relation. No dust continuum from GS-z14 is detected, suggesting an upper limit on the dust-to-stellar mass ratio of $< 2 \times 10^{-3}$, consistent with dust production from supernovae with a yield $y_d < 0.3 M_\odot$. Combining a previous JWST/MIRI photometric measurement of the [OIII]$\lambda\lambda$4959,5007Å and Hβ lines with Cloudy models, we find GS-z14 to be surprisingly metal-enriched ($Z \sim 0.05 - 0.2 Z_\odot$) a mere 300 Myr after the Big Bang. The detection of a bright oxygen line in GS-z14 thus reinforces the notion that galaxies in the early Universe undergo rapid evolution.

1. INTRODUCTION

The discovery and spectroscopic confirmation of galaxies at $z > 10$ has recently become possible due to the groundbreaking capabilities offered by the James Webb Space Telescope (*JWST*) (e.g. Curtis-Lake et al. 2023; Robertson et al. 2023; Bunker et al. 2023; Carniani et al. 2024; Finkelstein et al. 2024; Zavala et al. 2024). In particular JADES-GS-z14-0 (hereafter GS-z14) was recently spectroscopically confirmed to be the most distant known galaxy at $z_{\text{spec}} = 14.32^{+0.08}_{-0.20}$, less than 300 Myr after the Big Bang (Carniani et al. 2024). Notably GS-z14 is also very luminous with $M_{UV} = -20.81\pm0.16$, which makes it the second most luminous $z > 8$ galaxy with a spectroscopic redshift; only GN-z11 (Oesch et al. 2016; Bunker et al. 2023) is more luminous by a factor $\sim 2\times$.

Moreover, in contrast to other $z > 10$ galaxies, the rest-frame UV morphology of GS-z14 is extended and not highly concentrated. This implies that the luminosity is dominated by a spatially extended stellar population as opposed to an active galactic nucleus (AGN). The existence of objects like GS-z14 suggests a much more rapid build-up of galaxies in the very early universe than previously expected (Carniani et al. 2024). GS-z14 enables a unique opportunity to study this rapid build-up in detail (Ferrara 2024).

The high luminosity of GS-z14 makes it an exceptional target for multi-wavelength follow-up observations capable of revealing its physical conditions. Here we present new observations of GS-z14 targeting the luminous [OIII]$_{88\mu m}$ far-infrared line with the the Atacama Large Millimeter/submillimeter Array (ALMA).

The [OIII] 88-micron fine-structure line is one of the dominant coolants of the ISM. It originates from ionized gas in HII regions (Cormier et al. 2015), where ionizing radiation from young, massive stars has stripped electrons from oxygen atoms. Both semi-analytical models (Yang & Lidz 2020; Vallini et al. 2021, 2024) and radiative transfer post-processed large box (Moriwaki et al. 2018), cosmological zoom-in (Katz et al. 2017; Arata et al. 2020; Katz et al. 2022; Pallottini et al. 2022; Kohandel et al. 2023; Nakazato et al. 2023) hydrodynamical simulations have been employed to predict and interpret $[OIII]_{88\mu m}$ emission in high redshift sources. The consensus is that bright $[OIII]_{88\mu m}$ emission is generally associated with hard ionisation fields (Yang & Lidz 2020; Pallottini et al. 2022), high ionization parameters (Moriwaki et al. 2018; Arata et al. 2020; Vallini et al. 2024; Nakazato et al. 2023), and low metallicities (Katz et al. 2019; Vallini et al. 2024). These physical properties are likely to be ubiquitous in very actively star-forming galaxies at high redshifts, making this line the ideal target for ALMA follow-up observations of JWST-selected $z > 10$ galaxies.

In the last two years, ALMA follow-up observations have been performed for several high-redshift galaxy candidates. GHZ2 (Castellano et al. 2022; Naidu et al. 2022; Donnan et al. 2022; Harikane et al. 2023; Bouwens et al. 2023), with a photometric redshift of $z = 11.96 - 12.42$, was targeted with an ALMA Band 6 search for $[OIII]_{88\mu m}$ by Bakx et al. (2023), who determined a 5σ upper limit of $\log(L_{[OIII]}/L_\odot) < 1.7 \times 10^8$ (see also Popping 2023). GHZ2 was later spectroscopically confirmed at $z = 12.34$ (Castellano et al. 2024), with Zavala et al. (2024) estimating an SFR of $9 \pm 3\, M_\odot\, \mathrm{yr}^{-1}$ from the Hα line. Following its spectroscopic confirmation, Zavala et al. (2024) re-examined the ALMA observations of GHZ2 presented in Bakx et al. (2023), but were not able to identify a plausible $>5\sigma$ $[OIII]_{88\mu m}$ detection at the expected frequency.

An ALMA line scan was also performed on GHZ1, with a photometric redshift of $z \approx 10.6$ (Treu et al. 2023), SFR of $36.3^{+54.5}_{-26.8}\, M_\odot\, \mathrm{yr}^{-1}$ and stellar mass $\log(M_\star/M_\odot) = 9.1^{+0.3}_{-0.4}$ (Santini et al. 2023), yielding a marginal $[OIII]_{88\mu m}$ signal near its JWST position (Yoon et al. 2023) and an upper limit of $L_{[OIII]} < 2.2 \times 10^8\, L_\odot$ (5σ). Another high-redshift candidate, HD1 at $z = 13.3$ (Harikane et al. 2023) was observed in ALMA Bands 4 and 6 targeting $[CII]_{158\mu m}$ and $[OIII]_{88\mu m}$, respectively, but the lines were not detected (Kaasinen et al. 2023). HD1 was later shown to be a low-redshift interloper at $z = 4.0$ (Harikane et al. 2024). Finally, S5-z17-1, identified in JWST ERO data, showed a potential 5.1σ detection at 338.726 GHz, possibly corresponding to $[OIII]_{52\mu m}$ at $z = 16$ (Fujimoto et al. 2023), suggesting an SFR $< 120\, M_\odot\, \mathrm{yr}^{-1}$. However, the high-redshift nature of this galaxy has not been conclusively established.

Overall, these upper limits and non-detections indicate possible lower redshift solutions or insufficient sensitivity in the requested observations (Bakx et al. 2023; Furlanetto & Mirocha 2023; Kaasinen et al. 2023). However, the burstiness of SF in such high-redshift galaxies, as well as the impact of feedback processes on galaxy spectra and visibility, have also been suggested as physical motivations for the lack of ALMA detections at $z > 10$ (Nakazato et al. 2023; Kohandel et al. 2023).

Throughout this paper we assume a standard ΛCDM cosmology with $H_0 = 70$ km s^{-1} Mpc^{-1}, $\Omega_m = 0.3$ and $\Omega_\Lambda = 0.7$. Magnitudes are presented in the AB system (Oke & Gunn 1983). For star formation rates and stellar masses we adopt a Chabrier IMF (Chabrier 2003). Error-bars indicate the 68% confidence interval unless specified otherwise. All measured and derived physical quantities are corrected for gravitational lensing by a factor of $1.17\times$ (Carniani et al. 2024). Logarithms use base 10 unless specified otherwise.

2. OBSERVATIONS AND DATA-REDUCTION

2.1. *JWST*

GS-z14 was discovered in deep imaging of the GOODS-South field obtained by the JWST Advanced Deep Extragalactic Survey (JADES; Eisenstein et al. 2023a) and the First Reionization Epoch Spectroscopic COmplete Survey (FRESCO; Oesch et al. 2023). GS-z14 was initially flagged as a likely low redshift interloper (Hainline et al. 2024; Williams et al. 2024) due to a nearby foreground galaxy at $z = 3.475$ with a separation of only 0.4" and due to its high luminosity. However, further analysis including additional medium-band observations favored a high redshift solution (Robertson et al. 2023).

Deep follow-up spectroscopy with NIRSpec presented in Carniani et al. (2024) shows a strong break at $\sim 1.85\mu m$, consistent with a Lyman break at $z \sim 14$. The profile of the Lyman break is sensitive to absorption of hydrogen along the line of sight, neutral gas in the galaxy and environment, velocity offsets, the presence of Lyman alpha emission and possible ionized bubbles. Accounting for these effects, Carniani et al. (2024) determined a spectroscopic redshift of z = $14.32^{+0.08}_{-0.20}$.

In contrast to other $z > 10$ sources, the spectrum of GS-z14 does not contain strong rest-frame UV emission lines. Only CIII]$\lambda\lambda$1907,9Å is tentatively detected with a significance of 3.6σ at $z = 14.178 \pm 0.013$, consistent with the redshift obtained from the Lyman Break. Car-
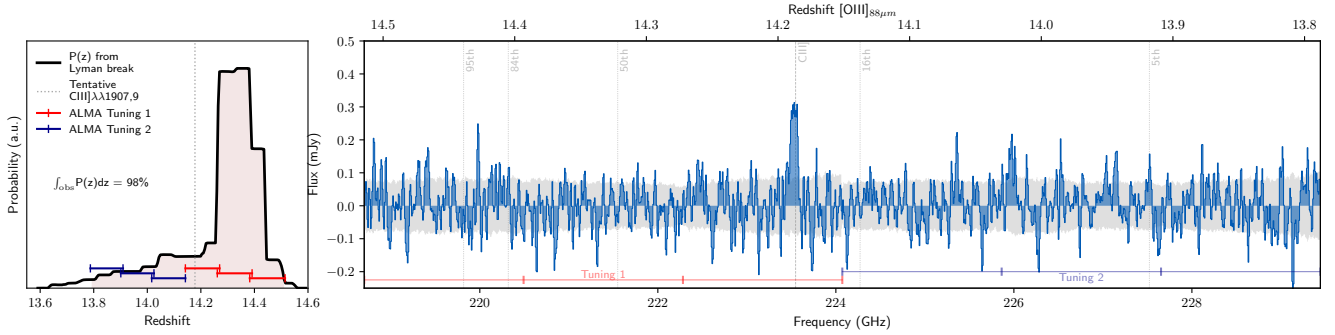
Figure 1. *Left Panel:* The ALMA observations cover 98% of the redshift probability distribution derived from the Lyman break as observed by NIRSpec PRISM. We use two tunings with three spectral windows each, tuning 1 and 2 cover 83% and 15% of the probability distribution respectively. *Right Panel:* Flux constraints extracted at the position of GS-z14 (*blue histogram*) vs. frequency from the 2023.A.00037.S spectral scan observations. The grey contours indicate the 1σ uncertainties. For context we show the expected redshift from the tentative CIII]$_{1907,1909}$ line from NIRSpec as well as the 5, 16, 50, 86 and 95th percentiles of the P(z) distribution. There is only one feature in the line scan that can be confidently identified as [OIII]$_{88\mu m}$ line emission and it occurs at a frequency of 223.528 ± 0.009 GHz.

niani et al. (2024) discuss a number of mechanisms that could be responsible for the lack of strong emission lines in the rest-frame UV, ranging from a sudden quenching of the star formation, very low or high metallicities ($Z<0.05Z_\odot$ or $Z\sim Z_\odot$), a high escape fraction of ionizing photons and a difference in the dominant ionizing flux.

Interestingly, GS-z14 is also detected by MIRI in the F770W filter (Helton et al. 2024). This filter covers the rest-frame optical emission of GS-z14, corresponding to wavelengths of 4.4 to 5.7μm. This part of the spectrum contains the strong [OIII]$\lambda\lambda4959,5007$Å and Hβ emission lines, and indeed the observed flux is significantly stronger than observed in the adjacent F444W filter, implying a significant contribution from the emission lines (constituting about 1/3 of the total F770W flux).

SED fitting of GS-z14 performed by Helton et al. (2024) shows that the photometry is consistent with a stellar mass of $\log(M_*/M_\odot)=8.7^{+0.5}_{-0.4}$. The models estimate that most of this stellar mass was formed relatively recently, with a mass-weighted age of ~20 Myr. Helton et al. (2024) determine the current (<10 Myr) star formation rate of GS-z14 to be 25^{+6}_{-5} M$_\odot$ yr^{-1}—consistent with the measurement of $22\pm6\,M_\odot$ yr^{-1} from Carniani et al. (2024). Combined with the measured size of 260 ± 20 pc, this implies a high star formation rate surface density of ~64 M$_\odot$ yr^{-1} pc^{-2}, comparable to intense starbursting galaxies in the local universe (Genzel et al. 2010). The UV slope $\beta_{UV}=-2.20\pm0.07$ indicates the presence of a moderate amount of dust in addition to the very young stellar population, with a visual extinction of $A_V=0.31^{+0.14}_{-0.07}$ (Carniani et al. 2024). Finally, the metallicity is poorly constrained owing to a lack of detected emission lines but is expected to be low ($Z = 0.014^{+0.052}_{-0.012}$ Z$_\odot$; Carniani et al. 2024).

2.2. *ALMA*

The ALMA Band 6 follow-up observations targeting the [OIII]$_{88\mu m}$ line were obtained as part of a Cycle 10 Director's Discretionary Time (DDT) program (#2023.A.00037.S, PI: Schouws). An observing set-up using two tunings with three spectral windows each was utilized to maximize the coverage of the redshift likelihood distribution derived from the spectroscopic Lyman break. This results in a continuous frequency coverage ranging from 218.70 GHZ to 229.45 GHz, corresponding to a redshift range of $z = 13.79$ to 14.51. We show in Figure 1 that the observing strategy covers 98% of the P(z).

The observations for Tuning 2 were carried out between 15 and 16 August 2024 in good weather conditions (PWV=0.67mm), achieving the requested sensitivity in 2.8 hours. Tuning 1 was observed between 7 and 8 September 2024 for 2.8 hours in excellent conditions (PWV=0.30mm). Both tunings were observed with different array configurations due to scheduling constraints. Tuning 1 was observed in C-4 and Tuning 2 in C-5 with baselines of $15-500$ and $15-919$ m, resulting in synthesized beams of $1.09'' \times 0.81''$ and $0.57'' \times 0.49''$ respectively when using natural weighting.

The ALMA data were reduced and calibrated following the standard ALMA pipeline procedures with the Common Astronomy Software Applications (v6.5.4-9) (Casa; Hunter et al. 2023). The amplitude and phase calibrations were performed using J0334-4008 and J0348-2749, respectively. Both calibrators are part of the ALMA Calibrator Source Catalogue and are therefore considered reliable for Band 6 observations. Under typical conditions, the absolute flux calibration accuracy for Band 6 is 5–10% (ALMA Technical Handbook 2024).

The data were well behaved, with no bad antennas or channels requiring flagging.

The resulting calibrated measurement sets were time-averaged in bins of 30 seconds to reduce the data-size, after carefully verifying that time-average smearing does not impact our results (e.g. Thompson et al. 2017).

Imaging of the calibrated visibilities was performed with natural weighting using the TCLEAN task in CASA, cleaning to a depth of 2σ using automasking (Kepley et al. 2020). We use a pixel scale of $0.076''$ to properly sample the synthesized beam, which has a FWHM of $1.08'' \times 0.80''$ at the frequency of the $[OIII]_{88\mu m}$ line.

2.3. Line Search

We perform a blind search for emission lines using an algorithm similar to the one used by Béthermin et al. (2020) for the ALPINE survey (Le Fèvre et al. 2020; Faisst et al. 2020) and Schouws et al. in prep. for the REBELS survey (Bouwens et al. 2022). The algorithm loops over all channels and collapses moment maps over a range of 75 to 350 km s^{-1} in steps of 1 channel ($\sim$10 km s^{-1}). For each moment map, we identify the significant ($>3\sigma$) peaks and add the results to a large list of features. This list is then pruned by removing duplicates within $2\times$FWHM and $1.5\times$ the beamsize. We also perform the search on the negative moment map, which is useful to characterize the noise properties. In Figure 1, we show a blind extraction of the ALMA spectrum at the location of GS-z14 using a 0.5" aperture.

The most significant line candidate we extract within a 0.5" radius of the JWST position of GS-z14 is detected with a peak significance of 6.6σ and separation of 0.12". The candidate line is consistent with being spatially coincident with GS-z14 in the JWST/NIRCam observations given expected 0.18" positional uncertainties following from a 6.6σ line detection and 1.08" beam.[1]

3. RESULTS

3.1. $[OIII]_{88\mu m}$ in GS-z14

We have identified an emission line with a signal-to-noise of 6.6σ within 0.12" of GS-z14 at 223.528±0.009 GHz. This corresponds to $[OIII]_{88\mu m}$ at $z = 14.1793 \pm 0.0007$, consistent with both the redshift derived from the Lyman break observed by JWST and also the tentative 3.6σ detection of $CIII]_{1907,1909}$ at $2.89\mu m$ (Carniani et al. 2024). In particular, the consistency of our new redshift determination from $[OIII]_{88\mu m}$ with the earlier redshift estimate $z = 14.178 \pm 0.003$ from the tentative $CIII]_{1907,1909}$ doublet (Carniani et al. 2024) greatly increases our confidence in the robustness of

the current redshift determination given the availability of multiple line detections. We show the contours of the $[OIII]_{88\mu m}$ emission overlaid on an RGB image based on F150W, F200W and F400W imaging and a S/N-optimized extraction of the spectrum in Figure 2.

We measure the integrated line flux using the moment-zero map of the emission line, including all channels that fall within $2\times$ the FWHM of the line. The FWHM is determined in an iterative process; starting from an estimate of the FWHM we collapse a moment-zero map and extract a 1d spectrum, which is extracted by including all pixels with S/N$>3\sigma$ on the moment-zero map. A new FWHM is then measured using this 1d spectrum by fitting a Gaussian. This new FWHM is then used to collapse a new moment-zero map for the next iteration. A stable FWHM is achieved in less than 10 steps (Schouws et al. 2022).

The final FWHM we measure is 136±31 km s^{-1}. Assuming that GS-z14 is dispersion-dominated and $r_{[OIII]}$ = r_e = 260 pc, this implies a dynamical mass of $(1.0\pm0.5)\times10^9$ $M_\odot(\sin i)^2$. At the current resolution we do not see evidence for a velocity gradient.

We measure an integrated flux of 39±10 mJy·km s^{-1} this corresponds to a $[OIII]_{88\mu m}$ luminosity of $(2.1 \pm 0.5) \times 10^8$ L$_\odot$ (Solomon et al. 1992) (after correction for lensing magnification; Carniani et al. 2024). This places GS-z14 a factor of $\sim 2\times$ below the local relation between L$_{[OIII]}$ and SFR for metal-poor dwarf galaxies from De Looze et al. (2014), albeit nearly within the scatter (Figure 3). The general consistency with the $z = 0$ relation for a galaxy a mere ~ 300 Myr after the Big Bang suggests that GS-z14 has undergone rapid evolution, as discussed in detail in Section 4.1.

3.2. Dust Continuum

We do not detect the dust continuum from GS-z14, with a formal $90\mu m$ continuum limit of $< 15.1\,\mu$Jy beam^{-1} (3σ). We provide an upper limit on its dust mass assuming an optically thin modified black body with a dust temperature of $T_d = 60$ K and $\beta_{IR} = 2.03$ for the dust SED. The assumed temperature is consistent with extrapolations from theoretical models (e.g., Liang et al. 2019; Sommovigo et al. 2022a) and observational trends (e.g., Schreiber et al. 2018; Faisst et al. 2020; Sommovigo et al. 2021, 2022a,b; Witstok et al. 2023a) to $z \approx 14$. We note that the precise evolution of dust temperature is still uncertain and debated (e.g. Sommovigo et al. 2022b). However, our assumption of a relatively high dust temperature is also supported by the inverse correlation between metallically and dust temperature noted by Sommovigo et al. (2022b) and in-

---

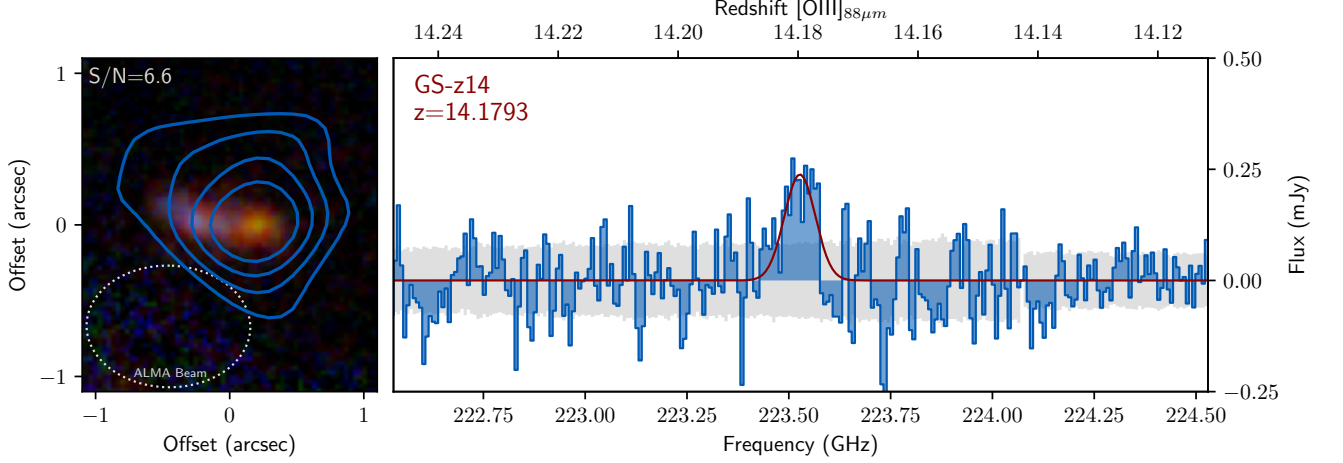[1] https://help.almascience.org/kb/articles/what-is-the-absolute-astrometric-accuracy-of-alma

Figure 2. Detection of [OIII]$_{88\mu m}$ in GS-z14 at $z = 14.1793 \pm 0.0007$. *Left Panel:* Contours showing the [OIII]$_{88\mu m}$ emission (2, 3, 4 and 5σ) overlaid on an RGB image based on F150W, F200W and F444W imaging (Eisenstein et al. 2023a,b). The object with a bluer colour to the left of GS-z14 is a z=3.475 foreground galaxy (Carniani et al. 2020). The [OIII]$_{88\mu m}$ emission is detected at a peak significance of 6.6σ in the collapsed data-cube and well centered on GS-z14. *Right Panel:* The spectrum of the [OIII]$_{88\mu m}$ line (*blue bars*) extracted from the $>3\sigma$ emission region in the moment-0 map. The red line shows the Gaussian fit used to measure the spectroscopic redshift and FWHM of the line. The grey shaded region indicates the 1σ uncertainties.
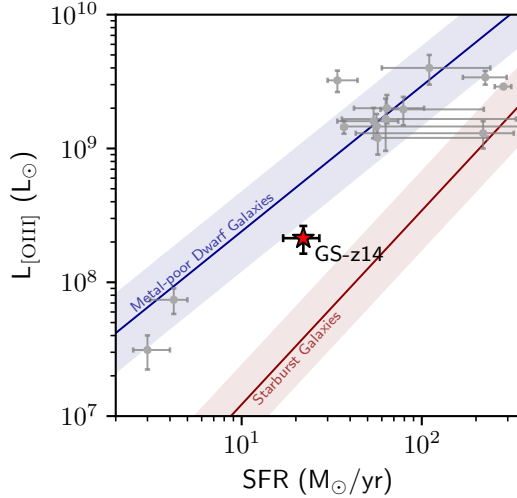
Figure 3. The luminosity of [OIII]$_{88\mu m}$ in GS-z14 is consistent with the local relation for metal-poor dwarf galaxies found by De Looze et al. (2014). For context we also show the local relation for starburst galaxies (De Looze et al. 2014) as well as a compilation of $z > 6.5$ galaxies (Bakx et al. 2020; Carniani et al. 2020; Harikane et al. 2020; Akins et al. 2022; Witstok et al. 2022; Algera et al. 2024; Fujimoto et al. 2024). Even as early as $z = 14.1793 \pm 0.0007$ and for high redshift galaxies in general, the relation for metal-poor dwarf galaxies seems to be a good fit (at SFR $\lesssim 100\,M_\odot\,\mathrm{yr}^{-1}$).

creasing temperature of the CMB background at high redshift[2].

We follow Ferrara et al. (2024) by adopting the Weingartner & Draine (2001) dust model with $\kappa_{88} = 34.15\,\mathrm{cm}^{-2}\,\mathrm{g}^{-1}$ at rest-frame 88 μm. This yields a (lensing-corrected) upper limit on the dust mass and infrared luminosity (integrated across $8 - 1000\,\mu$m) of $\log(M_\mathrm{d}/M_\odot) < 6.0$ and $\log(L_\mathrm{IR}/L_\odot) < 11.1$, respectively. The latter corresponds to an obscured SFR of $\mathrm{SFR_{IR}} < 14\,M_\odot\,\mathrm{yr}^{-1}$ which, combined with the unobscured SFR of GS-z14 inferred by Carniani et al. (2024), implies an obscured fraction of $f_\mathrm{obs} < 0.66$. Finally, using the stellar mass of GS-z14 inferred by Helton et al. (2024), we infer a dust-to-stellar mass ratio $\xi_d \equiv M_\mathrm{d}/M_\star < 1.9 \times 10^{-3}$.

The above estimates require the assumption of a dust temperature. Assuming a lower temperature of $T_\mathrm{d} = 45\,$K, which would imply no significant evolution of the dust temperature from $z \sim 4$ (e.g. Faisst et al. 2020), results in a dust mass of $\log(M_\mathrm{d}/M_\odot) < 6.8$. Meanwhile, a significantly higher temperature temperature of $T_\mathrm{d} = 100\,$K would result in a dust mass of $\log(M_\mathrm{d}/M_\odot) < 5.3$. In Section 4.2, we discuss this in further detail, focusing on the Attenuation Free Model by Ferrara et al. (2024) which self-consistently predicts a dust temperature for GS-z14 based on the observed V-band attenuation and the spatial extent of the dust.

---

[2] For context, the CMB background at $z = 14.2$ has a temperature of $T_\mathrm{CMB} = 41.4$K.
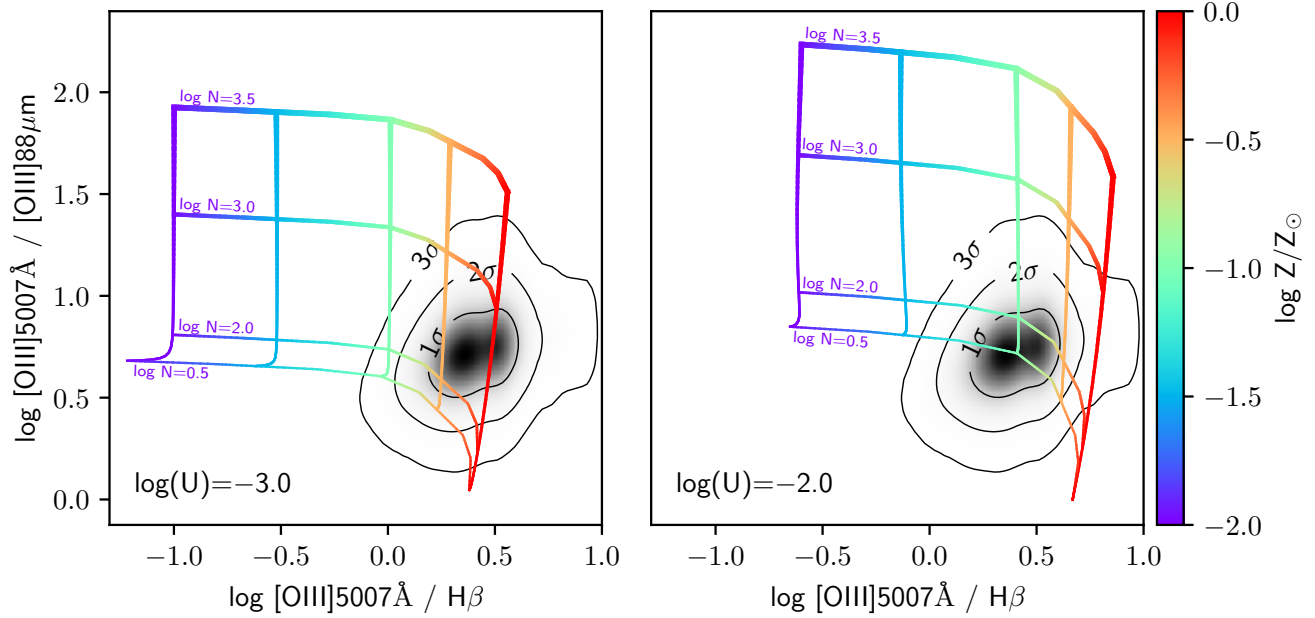
Figure 4. The ALMA and MIRI observations constrain the emission line ratios of GS-z14 to the dark shaded region in the figure highlighted by the 1 and 2σ contours. ISM modeling as shown by the coloured grid highlights the dependence on metallicity and density. This indicates that GS-z14 is consistent with a relatively high metallicity (Z>0.1 $Z_\odot$) and moderate to low density $\log(N) < 3.0 cm^{-3}$. There is a further minor dependence on the ionization parameter that shifts and deforms the grid, but does not impact the conclusions. For context, SED fitting of GS-z14 finds $\log(U) = -2.5 \pm 0.5$ (Helton et al. 2024).

4. DISCUSSION

4.1. Constraints on the ISM of GS-z14

Luminosity ratios of emission lines are invaluable diagnostic tools to probe the conditions of the ISM in galaxies. Although the NIRSpec spectroscopy of GS-z14 does not show significant emission lines, its detection in the MIRI F770W band places a constraint on the combined [OIII]λλ4959,5007Å+Hβ flux. Following Helton et al. (2024) we assume that the flux excess in F770W is 27.5±5.6 nJy based on a flat underlying continuum emission.

The [OIII]λ5007Å luminosity (hereafter [OIII]) can subsequently be calculated based on an assumed [OIII]/Hβ ratio and be compared to the luminosity of OIII as measured by ALMA. We repeat this calculation $10^6\times$, drawing random [OIII]/Hβ ratios from probability distribution from the SED fitting by Helton et al. (2024), where we combine the probability distributions from the three star formation history assumptions. This distribution has a median ratio of $2.5^{+0.9}_{-0.6}$. As noted by Helton et al. (2024), this is lower than the median [OIII]/Hβ at $z \sim 8.0$ which is $6.0^{+2.4}_{-2.9}$ in JADES (Helton et al. 2024), 6.4±0.9 in FRESCO (Meyer et al. 2024) and $7.2^{+2.6}_{-2.4}$ in PRIMAL (Heintz, K. E. et al. 2025).

In this process we also account for the uncertainty in the line luminosities from ALMA and JWST by drawing random values from a Gaussian error distribution.

The resulting constraints on the [OIII]/[OIII]$_{88\mu m}$ versus [OIII]/Hβ line ratios are shown in Figure 4. For context we show a grid of ISM models for a large range of conditions based on CLOUDY models (Ferland et al. 2017). The models consist of an HII region that smoothly transitions to a Photo Dissociation Region (PDR) until a fixed optical depth (A_V=10) in a plane parallel geometry. For more details on the model we refer to Witstok et al. (2022). We note that the ionization parameter of GS-z14 has been loosely constrained by Helton et al. (2024) to be $\log(U_{ion}) = -2.5 \pm 0.5$, and we therefore show two sets of CLOUDY models bracketing this range, at a fixed $\log(U_{ion}) \in (-3.0, -2.0)$. We focus on the grid with an ionization parameter $\log(U_{ion}) = -2$, as Kohandel et al. (2023) predict the most [OIII]$_{88\mu m}$-luminous galaxies at $z \gtrsim 10$ have high ionization parameters. Moreover, if the assumed [OIII]/Hβ is underestimated, the observed line ratios can only be reproduced by higher values of the ionization parameter.

While the uncertainties are substantial, given the existence of only a photometric detection of the [OIII]λλ4959,5007Å line, the Witstok et al. (2022) models suggest a relatively high metallicity of $Z \sim 0.1 Z_\odot$, in combination with a moderate-to-low electron density ($\log N \lesssim 10^{2.5}$). This is on the low end of, albeit still consistent with, the distribution of electron densities found for $z \gtrsim 5$ galaxies, which typically show values of $\log(N) \sim 2 - 3$ (e.g., Isobe et al. 2023). However, for

more accurate constraints on the ISM conditions of GS-z14, direct spectroscopic detections of additional oxygen lines are crucial, for example through MIRI spectroscopy.

Intriguingly, the detection of $[OIII]_{88\mu m}$ at $z = 14.1793 \pm 0.0007$ is consistent within 1σ with the tentative detection of CIII]$\lambda\lambda$1907,9Å reported by Carniani et al. (2024) at $z = 14.178 \pm 0.013$. Carniani et al. (2024) derive a CIII]$\lambda\lambda$1907,9Å rest-frame equivalent width (EW$_0$) of 8.0±2.3 Å, which is relatively high compared to the EW$_0$([OIII]+Hβ) of 370^{+360}_{-130} Å estimated by Helton et al. (2024), albeit consistent with the distribution found for galaxies at $z \sim 0-4$ (e.g. Maseda et al. 2017; Ravindranath et al. 2020; Tang et al. 2021), see Figure 5. The measured equivalent widths are in agreement with predictions from CLOUDY at a metallicity of $Z \sim 0.05 - 0.2\,Z_\odot$, and with an ionization parameter of $\log(U) \sim -2.5$, in agreement with Helton et al. (2024).

Moreover, Jones et al. (2020) derive a calibration for the oxygen abundance using the $[OIII]_{88\mu m}$ line and star-formation rate. Using their calibration we derive $12 + \log O^{++}/H^+ = 7.66^{+0.19}_{-0.21}$ (∼6-14% solar metallicity, using the solar abundance from Asplund et al. (2009)). In Figure 6 we use a CLOUDY grid with a 1Myr old input stellar population to estimate the $[OIII]_{88\mu m}$/SFR ratio as a function of ionisation parameter, for models with different metallicity and gas density. For modest gas density the measurements are consistent with 10% solar oxygen abundance, however, higher gas densities or older ages for the input stellar population will give higher metallicity estimates (up to solar metallicity).

The detection of both carbon and oxygen lines thus reinforce the notion that GS-z14 is already moderately chemically enriched. Adopting a fiducial $Z \sim 0.05 - 0.2\,Z_\odot$ in combination with the stellar mass from Helton et al. (2024), GS-z14 falls onto the high-redshift mass-metallicity relation, which has been mapped out to $z \sim 10$, and appears to show only mild evolution beyond $z \gtrsim 3$ (e.g., Curti et al. 2024).

4.2. *Constraints on Dust Formation Processes*

The build-up of dust in galaxies is a complex process involving multiple mechanisms of dust production and destruction, operating on different timescales. Supernova explosions (SNe) produce dust quickly, on timescales similar to the lifecycle of massive stars (∼10 Myr), whilst Asymptotic Giant Branch (AGB) stars contribute to dust production on significantly longer timescales (∼300 Myr, Schneider & Maiolino 2024). The contribution from grain growth in the ISM depends on the physical conditions, but is expected to be subdominant at extremely high redshifts and low gas-phase
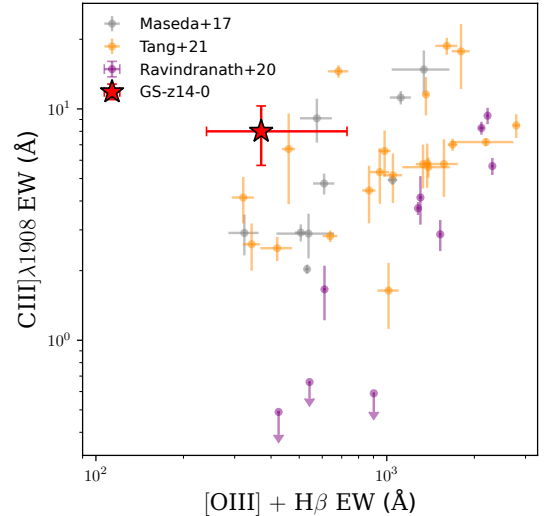

Figure 5. The rest-frame equivalent width of CIII]$\lambda\lambda$1907,9Å as a function of EW$_0$([OIII]+Hβ) (Carniani et al. 2024; Helton et al. 2024). GS-z14-0 is broadly consistent with measurements from the literature at $z = 1 - 3$ (grey, purple and orange points; Maseda et al. 2017; Ravindranath et al. 2020; Tang et al. 2021).
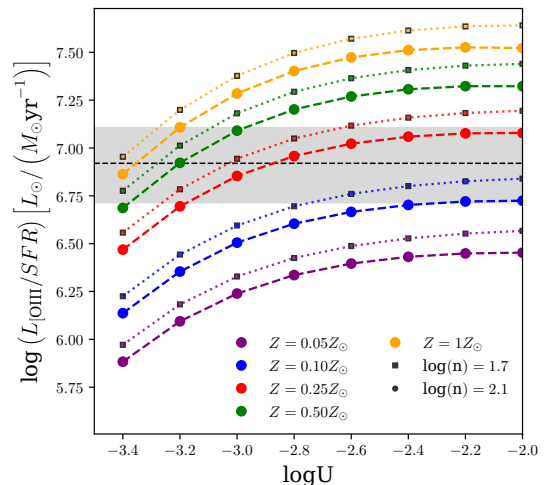

Figure 6. CLOUDY modelling of the $[OIII]_{88\mu m}$/SFR as a function of ionisation parameter for a range of metallicities and densities ∼50-100 cm^{-3}. Our model gives a lower limit on the metallicity of ∼10% $Z_\odot$, with higher gas densities and older ages preferring higher metallicity estimates.

metallicities (Ferrara et al. 2016; Dayal et al. 2022; Witstok et al. 2023a; Markov et al. 2024).

At lower redshifts it is difficult to disentangle the impact of different contributions (e.g., De Looze et al. 2020; Galliano et al. 2021), but GS-z14 has formed sufficiently early in cosmic history that dust production through SNe is likely the dominant formation process.

This makes GS-z14 an ideal test-bed for dust formation models in the early universe.

The efficiency of dust production from SNe can be inferred by measuring the dust-to-stellar mass ratio (ξ_d). This parameter is hard to interpret as it depends on both the expected number of SNe per unit of formed stellar mass (ν), which in turn depends on the assumed Initial Mass Function (IMF), and on the net dust yield per SN event (y_d), $\xi_d = y_d \times \nu$. In local SN remnants y_d values varying in the wide range from 0.01 to 1.1 $M_\odot$ have been directly measured (Milisavljevic et al. 2024). Such values are broadly in agreement with most indirect high-z measurements based on dust-to-stellar mass ratios (Sommovigo et al. 2022a,b).

Utilizing the continuum non-detection of GS-z14, we can attempt to place an upper limit on y_d. Following Michałowski (2015) and adopting a Salpeter IMF, the limit of $\xi_d < 2 \times 10^{-3}$ suggests a yield of $y_d < 0.24\,M_\odot/\mathrm{SN}$. This is consistent with a commonly adopted yield of $y_d \sim 0.1\,M_\odot/\mathrm{SN}$ (e.g., Sommovigo et al. 2022a; Dayal et al. 2022). If we rely on such a value for $y_d \sim 0.1\,M_\odot/\mathrm{SN}$ and assume that dust follows a similar spatial distribution as the stellar component, GS-z14 should be largely obscured ($A_V \sim 9.5$, see also Ferrara et al. 2024) and would not have been detected with JWST. However, the JWST data only reveal a relatively low visual extinction of $A_V = 0.31$, implying a much (1 dex) lower dust mass of $5 \times 10^4\,M_\odot$ with $\xi_d < 10^{-4}$ and $y_d < 0.015\,M_\odot/\mathrm{SN}$ (Ferrara et al. 2024).

Clearly, SNe (and later on growth in the ISM) do produce tangible amounts of dust, as less than 500 Myr later, at $z \approx 7$, dust appears widespread (Inami et al. 2022; Schouws et al. 2023; Witstok et al. 2023a; Algera et al. 2023) – both puzzlingly high dust-to-stellar mass ratios ($M_d/M_\star \sim 0.01$; Algera et al. 2024) and fully dust-obscured sources (Fudamoto et al. 2021) are observed at this epoch. In addition, features of the attenuation curve associated with the carbonaceous dust grains produced by SNe are observed at $z \sim 6.7$ (Witstok et al. 2023b).

The discrepancy between what is observed by JWST versus what is expected based on dust production from past SNe can be resolved by assuming that the majority of the dust has been removed from star-forming regions by radiation pressure-driven outflows. Such a scenario had been suggested in the Attenuation Free Model (AFM) presented in Ferrara et al. (2024).

In their fiducial model, Ferrara et al. (2024) suggest the dust in GS-z14 to have a typical extent of 1.4 kpc, as a more compact size would be inconsistent with the visual extinction measured by JWST. We note that, given the resolution of our data, dust of this extent would not be resolved across multiple ALMA beams. Combined with a fiducial yield of 0.1 $M_\odot/\mathrm{SN}$, the AFM predicts a continuum flux density for GS-z14 of $F_{88} = 14.9\,\mu$Jy. This is just below the sensitivity limit of our observations, which yield an upper limit of $F_{88} < 15.1\,\mu$Jy beam^{-1}. However, if the assumed dust yield is 0.5 dex lower ($0.1\,M_\odot/\mathrm{SN}$), then the expected flux density would be $F_{88} \sim 8\,\mu$Jy, well below the current limit. As such, a conclusive investigation of the dust content of GS-z14, as well as further testing of the AFM model predictions, requires deeper and high-resolution ALMA continuum observations.

Table 1. Properties of GS-z14

Parameter	Value
RA	03:32:19.9049
Dec	-27:51:20.265
Redshift	$z = 14.1793(7)$
M_{UV}	-20.81 ± 0.16
Stellar Mass ($\log(M_\odot)$)	$8.7^{+0.5}_{-0.4}$
Star Formation Rate ($M_\odot/\mathrm{yr}$)	25^{+6}_{-5}
[OIII]$_{88\mu m}$ Luminosity ($10^8\,\mathrm{L_\odot}$)	2.1 ± 0.5
FWHM [OIII]$_{88\mu m}$ (km s^{-1})	136 ± 31
Dynamical Mass ($M_\odot\,(\sin i)^2$)	$(1.0 \pm 0.5) \times 10^9$
90-μm continuum flux (μJy/beam)	< 15.1 (3σ)
Dust Mass ($\log(M_\odot)$)	< 6.0

Notes: M_{UV} from Carniani et al. (2024); stellar mass and SFR from Helton et al. (2024). Values have been corrected for a lensing magnification of $1.17\times$ (Carniani et al. 2024).

5. SUMMARY

We report the robust detection of a 6.6σ [OIII]$_{88\mu m}$ line of JADES-GS-z14-0 at 223.528 ± 0.009 GHz, providing us with a precise spectroscopic redshift measurement of $z = 14.1793 \pm 0.0007$. This represents a substantial jump in redshift over the previous high-redshift [OIII]$_{88\mu m}$-detection from MACS1149-JD1 at $z = 9.1096$ (Hashimoto et al. 2018). The [OIII]$_{88\mu m}$ line was identified using data from an ALMA Cycle-10 DDT program (2023.A.00037.S, PI: Schouws) providing a spectral scan from 218.70 to 229.45 GHz (10.75 GHz baseline), covering the redshift range z=13.79 to 14.51. The precision of the current redshift measurement represents $\gtrsim 180\times$ gain over the prior redshift measurement of $z = 14.32^{+0.08}_{-0.20}$ from NIRSpec.

The redshift we find for the source is consistent with the redshift Carniani et al. (2024) derive ($z = 14.178 \pm 0.013$) based on their tentative 3.6σ detection of CIII]$_{1907,1909}$ doublet at 2.89μm, providing strong evidence the earlier line detection is real. As such, we now

have multiple line detections of GS-z14-0, CIII]$_{1907,1909}$ (3.6σ) with JWST and [OIII]$_{88\mu m}$ (6.6σ) with ALMA, providing rather definitive evidence for the robustness of the redshift determination of GS-z14-0. Of note, the detection of [OIII]$_{88\mu m}$ with ALMA was achieved with less integration time (2.8 hours) than was required for the 3.6σ tentative detection of CIII]$_{1907,1909}$ with JWST (9.3 hours), providing a rather dramatic illustration of the discovery potential of ALMA.

We find no detection of the dust continuum from JADES-GS-z14-0 based on the DDT observations, with a $< 3\sigma$ upper limit of $<15.1\,\mu$Jy beam^{-1}. This suggests a low dust-to-stellar mass ratio of $M_{\rm d}/M_\star < 1.9 \times 10^{-3}$, consistent with supernova dust production yields $y_d < 0.24\,M_\odot$/SN.

Combining a previous JWST/MIRI photometric measurement of the [OIII]$\lambda\lambda$4959,5007Å and Hβ lines with CLOUDY models, we find GS-z14 to be surprisingly metal-enriched ($Z \sim 0.05$-$0.2\,Z_\odot$) a mere 300 Myr after the Big Bang, with moderate to low density $\log(N) < 3.0\,$cm^{-3}.

Thanks to the precise spectroscopic redshift measurement and [OIII]$_{88\mu m}$ line detection we now have for GS-14-0 using just 2.8 hours, it is clear that additional follow-up of GS-z14-0 with ALMA would be highly fruitful and should include (1) higher spatial resolution observations of [OIII]$_{88\mu m}$ to improve constraints on dynamical masses and state of GS-z14-0 and deeper constraints on the dust continuum, (2) observations of the [CII]$_{158\mu m}$ line in band 4, lying just 0.2 GHz above the low-frequency boundary, to better probe the ionization parameter U and build-up of metals, and (3) JWST/MIRI observations of [OIII]$\lambda\lambda$4959,5007Å and Hβ to place tighter constraints on the electron density and metallicity of GS-z14-0.

REFERENCES

Akins, H. B., Fujimoto, S., Finlator, K., et al. 2022, ApJ, 934, 64, doi: 10.3847/1538-4357/ac795b

Algera, H. S. B., Inami, H., Oesch, P. A., et al. 2023, MNRAS, 518, 6142, doi: 10.1093/mnras/stac3195

Algera, H. S. B., Inami, H., Sommovigo, L., et al. 2024, MNRAS, 527, 6867, doi: 10.1093/mnras/stad3111

ALMA Technical Handbook. 2024, ALMA Cycle 10 Technical Handbook, ALMA Observatory

Arata, S., Yajima, H., Nagamine, K., Abe, M., & Khochfar, S. 2020, MNRAS, 498, 5541, doi: 10.1093/mnras/staa2809

Asplund, M., Grevesse, N., Sauval, A. J., & Scott, P. 2009, ARA&A, 47, 481, doi: 10.1146/annurev.astro.46.060407.145222

Bakx, T. J. L. C., Tamura, Y., Hashimoto, T., et al. 2020, MNRAS, 493, 4294, doi: 10.1093/mnras/staa509

Bakx, T. J. L. C., Zavala, J. A., Mitsuhashi, I., et al. 2023, MNRAS, 519, 5076, doi: 10.1093/mnras/stac3723

Béthermin, M., Fudamoto, Y., Ginolfi, M., et al. 2020, A&A, 643, A2, doi: 10.1051/0004-6361/202037649

Bouwens, R., Illingworth, G., Oesch, P., et al. 2023, MNRAS, 523, 1009, doi: 10.1093/mnras/stad1014

Bouwens, R. J., Smit, R., Schouws, S., et al. 2022, ApJ, 931, 160, doi: 10.3847/1538-4357/ac5a4a

Bunker, A. J., Saxena, A., Cameron, A. J., et al. 2023, Astronomy & Astrophysics, 677, A88, doi: 10.1051/0004-6361/202346159

Bunker, A. J., Saxena, A., Cameron, A. J., et al. 2023, A&A, 677, A88, doi: 10.1051/0004-6361/202346159

Carniani, S., Ferrara, A., Maiolino, R., et al. 2020, MNRAS, 499, 5136, doi: 10.1093/mnras/staa3178

Carniani, S., Hainline, K., D'Eugenio, F., et al. 2024, Nature, 633, 318, doi: 10.1038/s41586-024-07860-9

Castellano, M., Fontana, A., Treu, T., et al. 2022, ApJL, 938, L15, doi: 10.3847/2041-8213/ac94d0

10

Castellano, M., Napolitano, L., Fontana, A., et al. 2024, ApJ, 972, 143, doi: 10.3847/1538-4357/ad5f88

Chabrier, G. 2003, PASP, 115, 763, doi: 10.1086/376392

Cormier, D., Madden, S. C., Lebouteiller, V., et al. 2015, A&A, 578, A53, doi: 10.1051/0004-6361/201425207

Curti, M., Maiolino, R., Curtis-Lake, E., et al. 2024, A&A, 684, A75, doi: 10.1051/0004-6361/202346698

Curtis-Lake, E., Carniani, S., Cameron, A., et al. 2023, Nature Astronomy, 7, 622, doi: 10.1038/s41550-023-01918-w

Dayal, P., Ferrara, A., Sommovigo, L., et al. 2022, Monthly Notices of the Royal Astronomical Society, 512, 989–1002, doi: 10.1093/mnras/stac537

Dayal, P., Ferrara, A., Sommovigo, L., et al. 2022, MNRAS, 512, 989, doi: 10.1093/mnras/stac537

De Looze, I., Cormier, D., Lebouteiller, V., et al. 2014, A&A, 568, A62, doi: 10.1051/0004-6361/201322489

De Looze, I., Lamperti, I., Saintonge, A., et al. 2020, MNRAS, 496, 3668, doi: 10.1093/mnras/staa1496

Donnan, C. T., McLeod, D. J., Dunlop, J. S., et al. 2022, Monthly Notices of the Royal Astronomical Society, 518, 6011–6040, doi: 10.1093/mnras/stac3472

Eisenstein, D. J., Willott, C., Alberts, S., et al. 2023a, arXiv e-prints, arXiv:2306.02465, doi: 10.48550/arXiv.2306.02465

Eisenstein, D. J., Johnson, B. D., Robertson, B., et al. 2023b, arXiv e-prints, arXiv:2310.12340, doi: 10.48550/arXiv.2310.12340

Faisst, A. L., Fudamoto, Y., Oesch, P. A., et al. 2020, Monthly Notices of the Royal Astronomical Society, 498, 4192, doi: 10.1093/mnras/staa2545

Faisst, A. L., Schaerer, D., Lemaux, B. C., et al. 2020, ApJS, 247, 61, doi: 10.3847/1538-4365/ab7ccd

Ferland, G. J., Chatzikos, M., Guzmán, F., et al. 2017, RMxAA, 53, 385. https://arxiv.org/abs/1705.10877

Ferrara, A. 2024, A&A, 689, A310, doi: 10.1051/0004-6361/202450944

Ferrara, A., Carniani, S., di Mascia, F., et al. 2024. https://arxiv.org/abs/2409.17223

Ferrara, A., Viti, S., & Ceccarelli, C. 2016, MNRAS, 463, L112, doi: 10.1093/mnrasl/slw165

Finkelstein, S. L., Leung, G. C. K., Bagley, M. B., et al. 2024, ApJL, 969, L2, doi: 10.3847/2041-8213/ad4495

Fudamoto, Y., Oesch, P. A., Schouws, S., et al. 2021, Nature, 597, 489, doi: 10.1038/s41586-021-03846-z

Fujimoto, S., Finkelstein, S. L., Burgarella, D., et al. 2023, ApJ, 955, 130, doi: 10.3847/1538-4357/aceb67

Fujimoto, S., Ouchi, M., Nakajima, K., et al. 2024, ApJ, 964, 146, doi: 10.3847/1538-4357/ad235c

Furlanetto, S. R., & Mirocha, J. 2023, Monthly Notices of the Royal Astronomical Society, 523, 5274–5279, doi: 10.1093/mnras/stad1799

Galliano, F., Nersesian, A., Bianchi, S., et al. 2021, A&A, 649, A18, doi: 10.1051/0004-6361/202039701

Genzel, R., Tacconi, L. J., Gracia-Carpio, J., et al. 2010, Monthly Notices of the Royal Astronomical Society, 407, 2091–2108, doi: 10.1111/j.1365-2966.2010.16969.x

Hainline, K. N., Johnson, B. D., Robertson, B., et al. 2024, ApJ, 964, 71, doi: 10.3847/1538-4357/ad1ee4

Harikane, Y., Ouchi, M., Inoue, A. K., et al. 2020, ApJ, 896, 93, doi: 10.3847/1538-4357/ab94bd

Harikane, Y., Ouchi, M., Oguri, M., et al. 2023, ApJS, 265, 5, doi: 10.3847/1538-4365/acaaa9

Harikane, Y., Ouchi, M., Oguri, M., et al. 2023, The Astrophysical Journal Supplement Series, 265, 5, doi: 10.3847/1538-4365/acaaa9

Harikane, Y., Inoue, A. K., Ellis, R. S., et al. 2024, arXiv e-prints, arXiv:2406.18352, doi: 10.48550/arXiv.2406.18352

Hashimoto, T., Laporte, N., Mawatari, K., et al. 2018, Nature, 557, 392, doi: 10.1038/s41586-018-0117-z

Heintz, K. E., Brammer, G. B., Watson, D., et al. 2025, AA, 693, A60, doi: 10.1051/0004-6361/202450243

Helton, J. M., Rieke, G. H., Alberts, S., et al. 2024. https://arxiv.org/abs/2405.18462

Hunter, T. R., Indebetouw, R., Brogan, C. L., et al. 2023, Publications of the Astronomical Society of the Pacific, 135, 074501, doi: 10.1088/1538-3873/ace216

Inami, H., Algera, H. S. B., Schouws, S., et al. 2022, MNRAS, 515, 3126, doi: 10.1093/mnras/stac1779

Isobe, Y., Ouchi, M., Nakajima, K., et al. 2023, ApJ, 956, 139, doi: 10.3847/1538-4357/acf376

Jones, T., Sanders, R., Roberts-Borsani, G., et al. 2020, ApJ, 903, 150, doi: 10.3847/1538-4357/abb943

Kaasinen, M., van Marrewijk, J., Popping, G., et al. 2023, A&A, 671, A29, doi: 10.1051/0004-6361/202245093

Katz, H., Kimm, T., Sijacki, D., & Haehnelt, M. G. 2017, MNRAS, 468, 4831, doi: 10.1093/mnras/stx608

Katz, H., Galligan, T. P., Kimm, T., et al. 2019, Monthly Notices of the Royal Astronomical Society, 487, 5902–5921, doi: 10.1093/mnras/stz1672

Katz, H., Rosdahl, J., Kimm, T., et al. 2022, MNRAS, 510, 5603, doi: 10.1093/mnras/stac028

Kepley, A. A., Tsutsumi, T., Brogan, C. L., et al. 2020, PASP, 132, 024505, doi: 10.1088/1538-3873/ab5e14

Kohandel, M., Ferrara, A., Pallottini, A., et al. 2023, MNRAS, 520, L16, doi: 10.1093/mnrasl/slac166

Le Fèvre, O., Béthermin, M., Faisst, A., et al. 2020, A&A, 643, A1, doi: 10.1051/0004-6361/201936965

Liang, L., Feldmann, R., Kereš, D., et al. 2019, MNRAS, 489, 1397, doi: 10.1093/mnras/stz2134

Markov, V., Gallerani, S., Ferrara, A., et al. 2024, arXiv e-prints, arXiv:2402.05996, doi: 10.48550/arXiv.2402.05996

Maseda, M. V., Brinchmann, J., Franx, M., et al. 2017, A&A, 608, A4, doi: 10.1051/0004-6361/201730985

Meyer, R. A., Oesch, P. A., Giovinazzo, E., et al. 2024, Monthly Notices of the Royal Astronomical Society, 535, 1067, doi: 10.1093/mnras/stae2353

Michałowski, M. J. 2015, A&A, 577, A80, doi: 10.1051/0004-6361/201525644

Milisavljevic, D., Temim, T., Looze, I. D., et al. 2024, The Astrophysical Journal Letters, 965, L27, doi: 10.3847/2041-8213/ad324b

Moriwaki, K., Yoshida, N., Shimizu, I., et al. 2018, Monthly Notices of the Royal Astronomical Society: Letters, 481, L84–L88, doi: 10.1093/mnrasl/sly167

Naidu, R. P., Oesch, P. A., van Dokkum, P., et al. 2022, ApJL, 940, L14, doi: 10.3847/2041-8213/ac9b22

Nakazato, Y., Yoshida, N., & Ceverino, D. 2023, ApJ, 953, 140, doi: 10.3847/1538-4357/ace25a

Oesch, P. A., Brammer, G., Dokkum, P. G. v., et al. 2016, The Astrophysical Journal, 819, 129, doi: 10.3847/0004-637x/819/2/129

Oesch, P. A., Brammer, G., Naidu, R. P., et al. 2023, MNRAS, 525, 2864, doi: 10.1093/mnras/stad2411

Oke, J. B., & Gunn, J. E. 1983, ApJ, 266, 713, doi: 10.1086/160817

Pallottini, A., Ferrara, A., Gallerani, S., et al. 2022, MNRAS, 513, 5621, doi: 10.1093/mnras/stac1281

Popping, G. 2023, Astronomy & Astrophysics, 669, L8, doi: 10.1051/0004-6361/202244831

Ravindranath, S., Monroe, T., Jaskot, A., Ferguson, H. C., & Tumlinson, J. 2020, The Astrophysical Journal, 896, 170, doi: 10.3847/1538-4357/ab91a5

Robertson, B. E., Tacchella, S., Johnson, B. D., et al. 2023, Nature Astronomy, 7, 611–621, doi: 10.1038/s41550-023-01921-1

Santini, P., Fontana, A., Castellano, M., et al. 2023, The Astrophysical Journal Letters, 942, L27, doi: 10.3847/2041-8213/ac9586

Schneider, R., & Maiolino, R. 2024, A&A Rv, 32, 2, doi: 10.1007/s00159-024-00151-2

Schouws, S., Stefanon, M., Bouwens, R., et al. 2022, ApJ, 928, 31, doi: 10.3847/1538-4357/ac4605

Schouws, S., Bouwens, R., Smit, R., et al. 2023, ApJ, 954, 103, doi: 10.3847/1538-4357/ace10c

Schreiber, C., Elbaz, D., Pannella, M., et al. 2018, A&A, 609, A30, doi: 10.1051/0004-6361/201731506

Solomon, P. M., Downes, D., & Radford, S. J. E. 1992, ApJL, 387, L55, doi: 10.1086/186304

Sommovigo, L., Ferrara, A., Carniani, S., et al. 2021, MNRAS, 503, 4878, doi: 10.1093/mnras/stab720

Sommovigo, L., Ferrara, A., Pallottini, A., et al. 2022a, MNRAS, 513, 3122, doi: 10.1093/mnras/stac302

Sommovigo, L., Ferrara, A., Carniani, S., et al. 2022b, MNRAS, 517, 5930, doi: 10.1093/mnras/stac2997

Tang, M., Stark, D. P., Chevallard, J., et al. 2021, MNRAS, 501, 3238, doi: 10.1093/mnras/staa3454

Thompson, A. R., Moran, J. M., & Swenson, George W., J. 2017, Interferometry and Synthesis in Radio Astronomy, 3rd Edition, doi: 10.1007/978-3-319-44431-4

Treu, T., Calabrò, A., Castellano, M., et al. 2023, The Astrophysical Journal Letters, 942, L28, doi: 10.3847/2041-8213/ac9283

Vallini, L., Ferrara, A., Pallottini, A., Carniani, S., & Gallerani, S. 2021, MNRAS, 505, 5543, doi: 10.1093/mnras/stab1674

Vallini, L., Witstok, J., Sommovigo, L., et al. 2024, MNRAS, 527, 10, doi: 10.1093/mnras/stad3150

Weingartner, J. C., & Draine, B. T. 2001, ApJ, 548, 296, doi: 10.1086/318651

Williams, C. C., Alberts, S., Ji, Z., et al. 2024, ApJ, 968, 34, doi: 10.3847/1538-4357/ad3f17

Witstok, J., Jones, G. C., Maiolino, R., Smit, R., & Schneider, R. 2023a, MNRAS, 523, 3119, doi: 10.1093/mnras/stad1470

Witstok, J., Smit, R., Maiolino, R., et al. 2022, MNRAS, 515, 1751, doi: 10.1093/mnras/stac1905

Witstok, J., Shivaei, I., Smit, R., et al. 2023b, Nature, 621, 267, doi: 10.1038/s41586-023-06413-w

Yang, S., & Lidz, A. 2020, Monthly Notices of the Royal Astronomical Society, 499, 3417–3433, doi: 10.1093/mnras/staa3000

Yoon, I., Carilli, C. L., Fujimoto, S., et al. 2023, The Astrophysical Journal, 950, 61, doi: 10.3847/1538-4357/acc94d

Zavala, J. A., Castellano, M., Akins, H. B., et al. 2024, arXiv e-prints, arXiv:2403.10491, doi: 10.48550/arXiv.2403.10491